From the middle stratosphere to the surface, using nitrous oxide to constrain the stratosphere-troposphere exchange of ozone

Daniel J. Ruiz[1] and Michael J. Prather[1]

[1]Department of Earth System Science, University of California, Irvine, CA 92697-3100, USA

Correspondence to: Daniel J. Ruiz (djruiz@uci.edu)

Abstract

Stratosphere-troposphere exchange (STE) is an important source of tropospheric ozone, affecting all of atmospheric chemistry, climate, and air quality. The study of impacts needs STE fluxes to be resolved by latitude and month, and for this we rely on global chemistry models, whose results diverge greatly. Overall, we lack guidance from model-measurement metrics that inform us about processes and patterns related to the STE flux of ozone (O_3). In this work, we use modeled tracers (N_2O, $CFCl_3$) whose distributions and budgets can be constrained by satellite and surface observations, allowing us to follow stratospheric signals across the tropopause. The satellite derived photochemical loss of N_2O on annual and quasi-biennial cycles can be matched by the models. The STE flux of N_2O-depleted air in our chemistry transport model drives surface variability that closely matches observed fluctuations on both annual and quasi-biennial cycles, confirming the modeled flux. The observed tracer correlations between N_2O and O_3 in the lowermost stratosphere provide a hemispheric scaling of the N_2O STE flux to that of O_3. For N_2O and $CFCl_3$, we model greater southern hemispheric STE fluxes, a result supported by some metrics, but counter to prevailing theory of wave-driven stratospheric circulation. The STE flux of O_3, however, is predominantly northern hemispheric, but evidence shows that this is caused by the Antarctic ozone hole reducing southern hemispheric O_3 STE by 14%. Our best estimate of the current STE O_3 flux based on a range of constraints is 400 Tg(O_3)/yr with a one-sigma uncertainty of ±15% and with a NH:SH ratio ranging from 50:50 to 60:40. We identify a range of observational metrics that can better constrain the modeled STE O_3 flux in future assessments.

1. Introduction & Background

The influx of stratospheric ozone (O_3) into the troposphere affects its distribution, variability, lifetime, and thus its role in driving climate change and surface air pollution (Zeng et al., 2010; Hess et al., 2015; Williams et al., 2019). The net stratosphere-to-troposphere exchange (STE) flux of O_3 has a regular seasonal cycle in each hemisphere that is an important part of the tropospheric O_3 budget (Stohl et al., 2003). Such fluxes are not directly observable, and we rely on observational estimates using trace-gas ratios, in particular the O_3:N_2O ratio in the lower stratosphere (Murphy and Fahey, 1994; McLinden et al., 2000), or dynamical calculations using measured/modeled winds and O_3 abundances (Gettelman et al., 1997; Olsen et al., 2004; Yang et al., 2016). The uncertainty in these estimates does not effectively constrain the wide range found in the models being used to project future ozone (Young et al., 2013, 2018; Griffiths et al., 2021). Here we present the case for using the observed variations in nitrous oxide (N_2O) from the middle stratosphere to the surface in order to constrain the STE flux of O_3. A similar case

47 has been made for the radionuclide [7]Be (Liu et al., 2016), but N_2O has a wealth of model-
48 observation metrics on hemispheric, seasonal, and interannual scales that constrains its STE flux
49 very well (Prather et al., 2015; Ruiz et al., 2021).
50
51 Ozone-rich stratospheric air has been photochemically aged and is depleted in trace gases such as
52 N_2O and chlorofluorocarbons (CFCs). For these trace gases, the overall circulation from
53 tropospheric sources to stratospheric destruction and back is part of the lifecycle that maintains
54 their global abundance (Holton, 1990). For N_2O and CFCs, this cycle of (i) loss in the middle to
55 upper stratosphere, (ii) transport to the lowermost stratosphere (Holton et al., 1995), and then (iii)
56 influx into the troposphere produces surface variations not related to surface emissions
57 (Hamilton and Fan, 2000; Nevison et al., 2004; Hirsch et al., 2006; Montzka et al., 2018; Ray et
58 al., 2020; Ruiz et al., 2021). In this work we relate our modeled STE fluxes to variations at the
59 surface and throughout the stratosphere, linking the fluxes of N_2O to O_3 through stratospheric
60 measurements. Our goal is to develop a set of model metrics founded on observations that are
61 related to the STE O_3 flux and can be used with an ensemble of models to determine a better,
62 constrained estimate for the flux, including seasonal, interannual, and hemispheric patterns. This
63 approach is similar to efforts involving the ozone depletion recovery time (Strahan et al.,
64 2011) and projections of future warming (Liang et al., 2020; Tokarska et al., 2020).
65
66 In a previous work (Ruiz et al., 2021, hence R2021) we showed that historical simulations with
67 three chemistry transport models (CTMs) were able to match the interannual surface variations
68 observed in N_2O. These were clearly driven by the stratospheric quasi-biennial oscillation
69 (QBO) which appears to be the major interannual signal in stratospheric circulation and STE
70 (Kinnersley and Tung, 1999; Baldwin et al., 2001; Olsen et al., 2019). In this work, we calculate
71 the monthly latitudinal STE fluxes of O_3, N_2O, and $CFCl_3$ (F11), establish a coherent picture
72 relating fluxes to observed abundances, and summarize the methods in Section 2. In section 3,
73 we examine the annual and interannual cycles as well as geographic patterns of modeled STE
74 flux. In section 4, we relate the surface variability of N_2O to its STE flux. We find some
75 evidence to support our model result that the STE flux of depleted-N_2O air is greater in the
76 southern hemisphere than in the northern, thus altering the asymmetry in surface emissions in the
77 source inversions (Nevison et al., 2007;Thompson et al., 2014). In section 5, we examine the
78 lowermost stratosphere to understand the large north-south asymmetry found in O_3 STE versus
79 N_2O or F11 STE, and find a clear signal of the Antarctic ozone hole in STE. In section 6, we
80 examine the consistency of the model calculations of STE flux and derive a best estimate for the
81 O_3 flux from this and previous studies. We summarize a sequence of model metrics, primarily
82 using O_3 and N_2O, that can narrow the range in the tropospheric O_3 budget terms for the multi-
83 model intercomparison projects used in tropospheric chemistry and climate assessments.
84
85 **2. Methods**
86
87 The modeled STE fluxes here are calculated with the UCI (University of California Irvine) CTM
88 driven by 3-hour forecast fields from the European Centre for Medium-range Weather Forecasts
89 (ECMWF) Integrated Forecast System (IFS Cycle 38r1 T159L60) for years 1990-2017, as are
90 the calculations in R2021. The CTM uses the IFS native 160x320 Gauss grid (~1.1°) with 60
91 layers, about 35 of which are in the troposphere. The stratospheric chemistry uses the linearized
92 model Linoz v3 and includes O_3, N_2O, NO_y, CH_4, and F11 as transported trace gases (Hsu and

Prather, 2010; Prather et al., 2015; Ruiz et al., 2021). There is no tropospheric chemistry, but rather a boundary-layer e-fold to a specified abundance, or a surface boundary reset to an abundance. Equivalent effective stratospheric chlorine levels are high enough to drive an Antarctic ozone hole, which is observed throughout this period. Thus, the ozone-hole chemistry in Linoz v3 is activated for all years, and the amount of O_3 depleted depends on the Antarctic meteorology of that year (Hsu and Prather, 2010).

The STE flux is calculated using the e90 definition of tropospheric grid cells (Prather et al., 2011) and the change in tropospheric tracer mass from before to after each tracer transport step as developed at UCI (Hsu et al., 2005; Hsu and Prather, 2009; Hsu and Prather, 2014). This method is precise and geographically accurate for O_3 and is self-consistent with a CTM's tracer-transport calculation (Tang et al., 2013; Hsu and Prather, 2014). Extensive comparisons with other methods of calculating STE are shown in Hsu and Prather (2014). Annual-mean STE fluxes are calculated from the full 28-year (336 month) time series as 12-month running means, and the annual cycle of monthly fluxes is the average of the 28 values for each month.

R2021 modeled the surface signal of stratospheric loss with the decaying tracers, N2OX and F11X (e.g., (Hamilton and Fan, 2000; Hirsch et al., 2006). These X-tracers have the identical stratospheric chemical loss frequencies as N_2O and $CFCl_3$, respectively, but no surface sources and are therefore affected only by the stratospheric sink and atmospheric transport. The multi-decade (F11X) to century (N2OX) decays are easily rescaled using a 12-month smoothing filter to give stationary results and a tropospheric mean abundance of 320 ppb. We treat F11X like N2OX with the same initial conditions and molecular weight. Budgets for N2OX are reported, as in N_2O studies (Tian et al., 2020), as Tg of N as N_2O. These rescaled N2OX and F11X tracers are designated simply as N2O (not N_2O) and F11. Our F11 STE fluxes are thus unrealistically large compared to current $CFCl_3$ fluxes, but can be easily compared with our N2O results.

When trying to calculate the STE flux of N_2O-depleted air across the tropopause, we found that the Hsu method was numerically noisy because the gradient across the tropopause, unlike that of O_3, was negligible. Thus, for this work we created the complementary tracers cN2OX and cF11X: for each kg of the X-tracer (i.e., N2OX) destroyed by photochemistry, 1 kg of its complementary tracer (cN2OX) is created. Air parcels that are depleted in N2OX (F11X) are therefore rich in cN2OX (cF11X). After crossing the tropopause, cN2OX and cF11X are removed through rapid uptake in the boundary layer, thus creating sharp gradients at the tropopause in parallel with that of O_3. As a check, we compared the boundary layer sinks of the c-tracers with their e90-derived STE fluxes and find that their sums are identical. The c-tracers and their STE fluxes are rescaled as are the X-tracers to give them a stationary time series corresponding to a tropospheric abundance of 320 ppb for their parallel X tracers. We designate these scaled tracers simply as cN2O and cF11.

3. Modeled STE fluxes

3.1 Global and hemispheric means

The 28-year mean of global O_3 STE is 390±16 Tg/yr (positive flux means stratosphere to troposphere, the ± values are the standard deviation of the 28 annual means and do not represent

139 uncertainty). This value is well within the uncertainty in the observation-based estimates
140 (Murphy and Fahey, 1994; Olsen et al., 2001), and far from the extreme ranges of the 34 models
141 in the latest Tropospheric Ozone Assessment Report (Young et al., 2018), 150 to 940 Tg/yr. The
142 global STE flux of cN2O is 11.5 ± 0.7 Tg/yr, and that of cF11 is 23.5 ± 1.5 Tg/yr. These fluxes for
143 cN2O and cF11 match the total long-term troposphere-to-stratosphere flux of N2O and F11 as
144 derived from their stratospheric losses. The cF11 budget is about twice as large as cN2O,
145 because F11 is photolyzed rapidly in the lower-middle stratosphere (~24 km) instead of the
146 upper stratosphere like N2O (~32 km). The seasonal mean pattern of STE fluxes are shown in
147 Figure 1. The large majority of STE flux enters the troposphere at 25°-45° latitude in each
148 hemisphere, but there is a broadening of the northern flux to 65°N in Jun-Jul. The importance of
149 this region about the sub-tropical jet for STE is supported by satellite data where stratospheric
150 folding events (high O_3 in the upper troposphere) are found at the bends of the jet (Tang and
151 Prather, 2010).
152
153 Given the small STE fluxes in the core tropics, the northern hemisphere (NH) and southern
154 hemisphere (SH) fluxes are distinct. The annual mean of NH O_3 STE is 208 ± 11 Tg/yr and is
155 slightly larger than the SH mean of 182 ± 11 Tg/yr. This NH:SH ratio of 53:47 is typically found
156 in other studies (Gettelman et al., 1997; Hsu and Prather, 2009; Yang et al., 2016), although
157 some have higher ratios like 58:42 (Hegglin and Shepherd, 2009; Meul et al., 2018). In contrast,
158 for cN2O and cF11, the NH flux (5.1 ± 0.4 Tg/yr and 10.6 ± 0.8 Tg/yr, respectively) is smaller than
159 the SH flux (6.4 ± 0.5 Tg/yr and 12.9 ± 1.0 Tg/yr, respectively), giving a NH:SH ratio of about
160 45:55. The established view on STE is that the flux is wave-driven and under downward control,
161 and thus the NH flux is much greater than the SH flux (see Table 1 of Holton et al., 1995; also
162 Appenzeller et al., 1996). Our unexpected results require further analysis including evidence for
163 hemispheric asymmetry in observations which is shown in section 4 along with other model
164 metrics.
165
166
167
168
169
170
171
172

(a)

(b)

(c)

Figure 1. The seasonal (latitude by month) cycle of STE flux (Tg/yr) for **(a)** O₃, **(b)** cN2O, and **(c)** cF11. Each month is averaged for years 1990-2017 (e.g., the 28 Januarys are averaged). The colorbar units are % of global, annual mean STE in each bin (1 month by ~1.1° latitude).

173
174
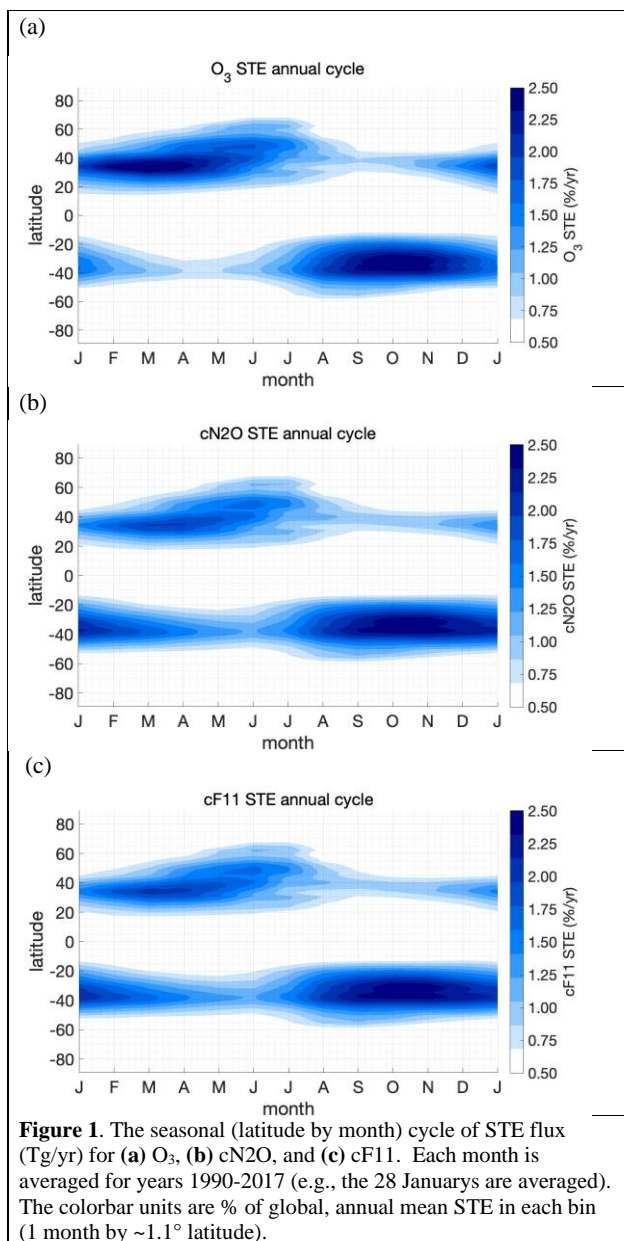
175 *3.2 Seasonal cycle*
176
177 The seasonal cycles of STE fluxes summed over global, NH, and SH are shown in Figure 2. The
178 scales are given as the annual rate (as if the monthly rate were maintained for the year), and each
179 species has a different axis. The right y-axes are kept at a N2O:F11 ratio of 1:2. Despite large
180 differences in the stratospheric chemistry across all three species, the seasonal cycle of STE is
181 highly correlated (Pearson's correlation coefficient cc > 0.98, except for SH O_3), indicating that
182 all three enter the troposphere from a seasonally near-uniform mixture of O_3:N2O:F11 in the
183 lowermost stratosphere.
184
185 Global STE peaks in June and reaches a minimum in November. The two hemispheres have
186 dramatically different seasonal amplitudes and somewhat opposite phases. NH peak STE for all
187 3 species occurs in the late boreal spring (May-June), while that in the SH occurs at the start of
188 austral spring (September-October). In the NH O_3 STE peaks a month before the c-tracers, and
189 in the SH the whole annual cycle of O_3 is shifted a month earlier. The NH STE seasonal
190 amplitude is very large for all species (~ 4:1 ratio max-to-min) with exchange almost ceasing in
191 the fall. In contrast, the SH STE is more uniform year-round with a 1.5:1 ratio for cN2O and
192 cF11, and 2.2:1 for O_3. Other models with similar NH and SH O_3 fluxes show different seasonal
193 amplitudes and phasing (see Fig. 6 of Tang et al., 2021), which will affect tropospheric O_3
194 abundances. It is important to develop observational metrics that test the seasonality of the
195 lowermost stratosphere related to STE fluxes, and to establish monthly STE fluxes as a standard
196 model diagnostic.
197
198 An interesting result here is the very tight correlation of the monthly cN2O and cF11 STE while
199 the O_3 STE is sometimes shifted. Loss of N_2O and F11 occurs at very different altitudes in the
200 tropical stratosphere (~32 km and ~24 km, respectively), but both have similar seasonality in
201 loss, driven mostly by the intensity of sunlight along the Earth's orbit (N_2O loss peaks in Feb and
202 reaches a minimum in July, see Fig. 4 from Prather et al. (2015). Photochemical losses of N_2O
203 and F11 drop quickly for air descending from the altitudes of peak loss in the tropics and hence
204 the relative cN2O and cF11 STE fluxes are locked in. O_3, however, continues to evolve
205 photochemically from 24 km to 16 km (upper boundary of the lowermost stratosphere), through
206 net photochemical production in the tropics and loss at mid- and high-latitudes that depends on
207 sunlight and is thus seasonal. There may be observational evidence for the patterns modeled
208 here in the correlation of these three tracers in the lower (16-20 km) and lowermost (12-16 km)
209 extratropical stratosphere (see section 4).
210

Figure 2. The annual cycle of monthly STE (Tg/yr) of O_3 (black lines), cN2O (orange lines), and cF11 (blue lines). **(a)** Global STE fluxes, and **(b)** hemispheric STE fluxes (NH, solid lines; SH, dashed lines). Each month is averaged for years 1990-2017 (e.g., the 28 Januarys are averaged). Note the different y-axes for each tracer in each panel.
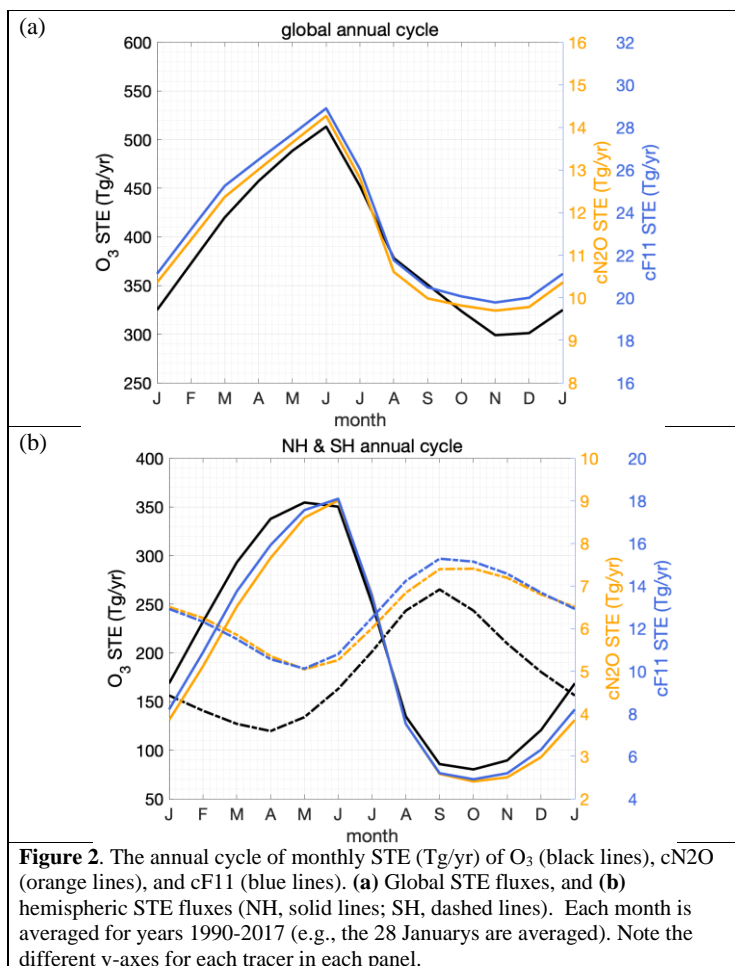
211
212
213 ### *3.3 Interannual variability*
214
215 Interannual variability (IAV) of N_2O loss and its lifetime is associated primarily with the QBO
216 (most recently, R2021). When the QBO is in its easterly (westerly) phase the entire overturning
217 circulation is enhanced (suppressed) (Baldwin et al., 2001). This results in more (less) air rich in
218 N_2O and F11 being transported from the troposphere to the lower or middle stratosphere, thereby
219 increasing (decreasing) the N_2O and F11 sinks (Prather et al., 2015; Strahan et al., 2015). From
220 the tropical stratosphere, the overturning circulation transports air depleted in N_2O and F11 into
221 the lowermost extratropical stratosphere, where it enters the troposphere. R2021 showed that the

222 observed surface variability of N_2O from this circulation can be modeled and has a clear QBO
223 signal, but one that is not strongly correlated with the QBO signal in stratospheric loss.
224
225 We generate the IAV of STE fluxes for O_3, cN2O, and cF11 in Figure 3abc with panels for
226 global, NH, and SH. Values are 12-month running means, and so the first modeled point at
227 1990.5 is the sum of STE for Jan through Dec of 1990. In Figures 3bc, we also show the
228 seasonal amplitude of STE with double-headed arrows on the left (O_3) and right (cN2O and
229 cF11). In a surprising result, the large NH-SH differences in seasonal amplitude are not reflected
230 in the IAV where NH and SH amplitudes are similar for all three tracers. The QBO modulation
231 of the lowermost stratosphere and STE appears to be unrelated to the seasonal cycle in STE.
232
233 Global STE for all three tracers shows QBO-like cycling throughout the 1990-2017 time series:
234 cN2O and cF11 are well correlated (cc ~ 0.9), but either species with O_3 is much less so (cc <
235 0.7). The hemispheric breakdown provides key information regarding O_3. In the NH the STE
236 IAV is similar across all three tracers with high correlation coefficients (cc = 0.82 for O_3-cN2O,
237 0.83 for O_3-cF11, and 0.94 for cN2O-cF11). Conversely in the SH, O_3 STE diverges from the c-
238 tracer fluxes, showing opposite-sign peaks in 2003 and 2016. The corresponding SH
239 correlations are (cc = 0.38, 0.65. 0.85). The loss of correlation between cN2O and cF11 is
240 unusual: cN2O STE drifts downward relative to cF11 STE, particularly after 2007; nevertheless,
241 the fine structure after 2007 is well matched in both tracers.
242
243 In the SH, the massive loss of O_3 within the Antarctic vortex, when mixed with the extra-polar
244 lowermost stratosphere will systematically shift the O_3 STE to lower values, with less impact on
245 the cN2O and cF11 STE. The IAV of the Antarctic winter vortex, in terms of the amount of O_3
246 that is depleted (see Fig. 4-4 of WMO, 2018), appears to drive the decorrelation of the SH STE
247 fluxes and is analyzed in section 4.
248
249 In the NH, the high variability of the Arctic winter stratosphere can modulate the total O_3 STE
250 flux (e.g., Hsu and Prather, 2009) but appears to maintain the same relative ratio with the cN2O
251 and cF11 fluxes. Model results here indicate that in the NH, the IAV of O_3, cN2O, and cF11 STE
252 fluxes are synchronized, and thus the air masses entering the lowermost stratosphere have the
253 same chemical mixtures from year to year. We know that cold-temperature activation of
254 halogen-driven O_3 depletion in the Arctic winter at altitudes above 400 K (potential temperature)
255 can produce large IAV in column ozone (Manney et al., 2011); but the magnitude is still much
256 smaller than in the Antarctic; and it may not reach into the lowermost stratosphere (<380K
257 potential temperature). This model accurately simulates Antarctic O_3 loss (section 4), but we
258 have not evaluated it for Arctic loss, and the Arctic conditions operate closer to the thresholds
259 initiating loss where Linoz v3 chemistry may be inadequate. The same meteorology and
260 transport model with full stratospheric chemistry is able to simulate Arctic O_3 loss (Oslo's
261 CTM2: Isaksen et al., 2012), and thus it will be possible to re-evaluate the NH IAV with such
262 models or with lowermost stratosphere tracer measurements.
263
264
265
266
267

Figure 3. (a) Global STE (Tg/yr), calculated at e90 tropopause, of O₃ (black line; left y-axis), cN2O (orange line; orange right y-axis), and cF11 (blue line; blue right y-axis) for years 1990-2017. Values are 12-month running means, and so the first point at 1990.5 is the sum of STE for Jan through Dec of 1990. **(b)** NH STE. **(c)** SH STE. The scales for cN2O and cF11 are kept in a 1:2 ratio. The asterisks and vertical double-headed arrows (**b** & **c**) depict the seasonal mean and amplitude for each species in each hemisphere.

268
269

270 *3.4 The link from stratospheric loss to STE flux*
271
272 What is unusual about the very tight correlation of cN2O and cF11 STE fluxes is that the
273 photochemical loss of N2O and F11 occurs at very different altitudes in the tropical stratosphere,
274 which are not in phase with respect to the QBO as shown in R2021 (their Fig. 2). The separate
275 phasing of cN2O and cF11 production is lost, presumably by diffusive tracer transport, by the
276 time they reach the extratropical lowermost stratosphere. The overall synchronization of the
277 STE fluxes implies that the absolute STE flux is driven primarily by variations in venting of the
278 lowermost stratosphere as expected (Holton et al., 1995; Appenzeller et al., 1996) rather than by
279 variations in the chemistry of the middle stratosphere.
280
281 This disconnect between the chemical signals generated by the prominent QBO signature of
282 wind reversals, upwelling in the tropical stratosphere, and the STE fluxes is also clear in the
283 magnitude of the loss versus STE. For N$_2$O, the IAV of cN2O production has a range of ±0.5
284 Tg/yr, whether from Microwave Limb Sounder (MLS) observations or the model; whereas the
285 IAV of cN2O STE flux is ±1.1 Tg/yr. The same is true in relative terms for cF11. Thus, the
286 modulation of the lowermost stratosphere by the QBO is clearly a part of the overall changes in
287 stratospheric circulation related to the QBO (Tung and Yang, 1994a; Kinnersley and Tung,
288 1999) and is the dominant source of IAV for these three greenhouse gases.
289
290 *3.5. The QBO signal*
291
292 To examine the QBO cycle in STE flux, we build a composite pattern (see R2021, Fig. 3 of N$_2$O
293 surface variations), by synchronizing the STE IAV in Figure 2 with the QBO cycle. The sync
294 point (offset = 0 months) is taken from one of the standard definitions of the QBO phase change,
295 i.e., the shift in sign of the 40-hPa tropical zonal wind from easterly to westerly (Newman,
296 2020). The 1990-2017 model period has 12 QBO cycles, but we restrict our analysis here to
297 years 2001-2016 to overlap with the observed surface N$_2$O data. This period includes seven
298 QBO phase transitions (01/2002, 03/2004, 04/2006, 04/2008, 08/2010, 04/2013, 07/2015), but
299 the observed surface N$_2$O is highly anomalous during the QBO centered on 08/2010 (R2021), so
300 we remove it from our comparison for consistency with R2021 (see their Fig S4d). The resulting
301 QBO composites for NH and SH in Figure 4 span 28 months.
302
303 In the NH, the QBO modulation of all three tracers is similar: STE flux begins to increase at an
304 offset of -8 months and continues to increase slowly for a year, peaking at an offset of +4
305 months; thereafter it decreases more rapidly in about ½ year (offset = +10). The rise-and-fall
306 cycle takes about 18 months. In the SH, the pattern for cN2O and cF11 is more sinusoidal and is
307 shifted later by ~3 months. The SH amplitude of the c-tracers is slightly larger relative to the
308 hemispheric mean flux than in the NH, and thus the SH QBO signal is larger than the NH by
309 about 40%. Thus, over the typical QBO cycle centered on the sync point, more depleted N$_2$O
310 and F11 is entering the SH than in the NH. For O$_3$, the SH modulation of STE is irregular and
311 reduced compared with the NH. Our hypothesis here, consistent with the annual cycle of STE
312 (Figure 1), is that the breakup of the Antarctic ozone hole has a major impact on STE,
313 particularly that of O$_3$, and that its signal has large IAV that does not synchronize with the QBO.
314 Surprisingly, the large wintertime IAV in the NH Arctic, in the form of sudden stratospheric
315 warmings, does not seem to have a major role in STE fluxes as noted above. This model may

316 miss some of the Arctic O_3 depletion, but it accurately simulates the warmings, which must have
317 a small impact on STE because they do not disrupt the clear QBO signal in the c-tracers.
318
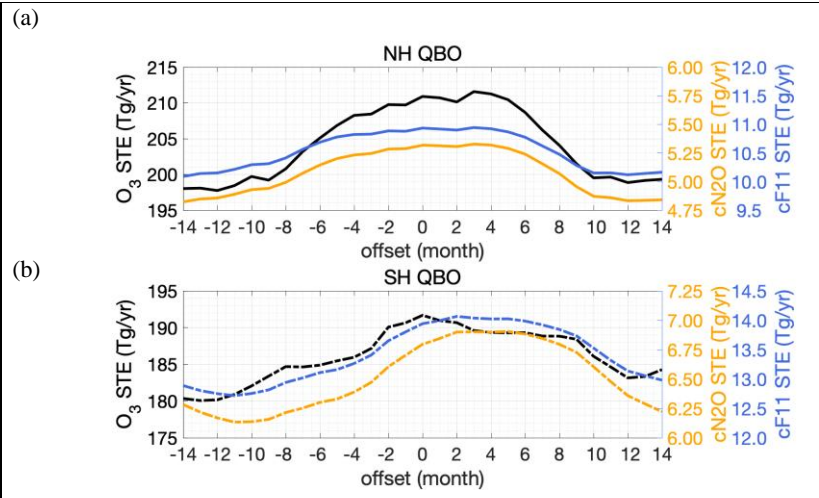
Figure 4. QBO composites of the STE of O_3 (black lines; left y-axes), cN2OX (orange
lines; orange right y-axes), and cF11X (blue lines; blue right y-axes) for the **(a)** NH (0°-
90°N; solid lines) and **(b)** SH (0°-90°S; dashed lines). These composites are averages
centered on the QBO phase transition at 40 hPa throughout the period of surface
observations (years 2001-2016, excluding the 08/2010 observed anomaly, for a total of 6
QBOs). Note: the y-axes limits are different for each panel, but the interval scale is
consistent for each tracer.

319
320
321   **4. Surface variability of N_2O related to STE flux**
322
323 Surface variability of N_2O is driven by surface emissions, stratospheric loss, and atmospheric
324 transport that mixes the first two signals. R2021 explored the variability originating only from
325 stratospheric chemistry using the decaying tracer N2OX. Here, we use surf-N2O to denote the
326 surface abundances of N2OX when corrected to steady state. R2021 showed that three
327 independent chemistry-transport models produced annual and QBO patterns in surface N_2O
328 simply from stratospheric loss. In this paper we link surf-N2O to the STE cN2O flux, which is
329 linked above to the STE O_3 flux.
330
331 The observed surface N_2O, denoted obs-N_2O and taken from the NOAA network (Dlugokencky
332 et al., 2019), shows a slowly increasing abundance (~0.9 ppb/yr) with a clear signal of annual
333 and interannual variability at some latitudes (see R2021). We calculate annual and QBO-
334 composite obs-N_2O after de-trending and restrict analysis in this section to model years 2001-
335 2016 to be consistent with the surface data. The latitude-by-month pattern of obs-N_2O includes
336 the impact of both stratospheric loss (~13.5 Tg/yr) and surface emissions (~17 TgN/yr), with the
337 preponderance of emissions being in the NH (Tian et al., 2020). Total emissions are not

338 expected to have large IAV but may have a seasonal cycle. The seasonal variation of surface
339 N$_2$O can also be driven by seasonality in the interhemispheric mixing of the NH-SH gradient (~1
340 ppb).
341
342
343 *4.1 Annual cycle*
344
345 Figure 5 replots the hemispheric mean annual cycles of cN2O STE flux alongside the annual
346 cycles of surf-N2O and obs-N$_2$O. As noted above, the STE in each hemisphere is almost in
347 opposite phase, as is the modeled surf-N2O (taken from Fig. 5 of R2021). The NH:SH
348 amplitude ratio is about 2.4:1 for both STE and surf-N2O. The lag from peak STE flux of cN2O
349 (negative N$_2$O) to minimum surf-N2O is about 3 months. Such a 90° phase shift is expected for
350 the seasonal variation of a long-lived tracer relative to a seasonal source or sink. The time lag
351 between the signal at the tropopause and at the surface, the tropospheric turnover time, should be
352 no more than a month. Surprisingly, the cN2O STE seasonal amplitude is much larger in the NH
353 (±3.4 Tg/yr) than in the SH (±1.3 Tg/yr), although the SH mean (6.5 Tg/yr) is larger than the NH
354 (5.2 Tg/yr). Essentially, there is more variability of air depleted in N$_2$O entering the NH, but air
355 entering the SH has a larger overall deficit. Thus in our model, the stratosphere creates a NH-SH
356 gradient of +0.3 ppb at the surface, which is a significant fraction of the observed N-S difference
357 of +1.3 ppb (R2021). This important result needs to be verified with other models or analyses
358 because it constrains the NH-SH location of sources.
359
360 In the NH, as noted in R2021, the two surface abundances, surf-N2O and obs-N$_2$O, have the
361 same amplitude and phase, implying that, if the model is correct, the emissions-driven surface
362 signal has no seasonality, although we know that some important emissions are seasonal
363 (Butterbach-Bahl et al., 2013). In the SH, the surf-N2O signal is much smaller, in parallel with
364 the small seasonal amplitude in cN2O STE, but it is out of phase with the obs-N$_2$O. This result
365 implies that the SH has some highly seasonal sources, or simply that the forcing of SH surf-N2O
366 by the seasonal cycle of cN2O is weak. Indeed, this is what we might expect from Figure 3: In
367 the NH the seasonal amplitude in N$_2$O overwhelms the IAV amplitude and is driving the obs-
368 N$_2$O; but in the SH, both amplitudes are comparable. Given the quasi-regular nature of the
369 QBO, it would interfere with the seasonal cycle and likely change its phase (as found for other
370 models in R2021).
371
372 In the NH, the annual cycle of O$_3$ and cN2O STE are clearly linked. If we accept that the obs-
373 N$_2$O NH seasonal cycle is simply driven by the STE flux, then how will tropospheric O$_3$ respond
374 seasonally? A mole-fraction scaling of the STE fluxes gives an O$_3$:N$_2$O ratio of ~25, and thus
375 scaling the surf-N2O amplitude gives a large O$_3$ surface seasonality of ~18 ppb. However, the
376 residence time of a tropospheric O$_3$ perturbation is ~1 month, and thus the peak surface
377 abundance will lag the peak STE flux by only about a month and not by 3 months as for N$_2$O.
378 O$_3$ will equilibrate with the flux on monthly timescales and not accumulate. Thus, our estimate
379 is that NH 30°-90° surface ozone might increase about 5 ppb, peaking in June, due to the STE
380 flux. In the SH, seasonal patterns are weaker and not well defined, and thus no obvious STE O$_3$
381 signal is expected.
382
383
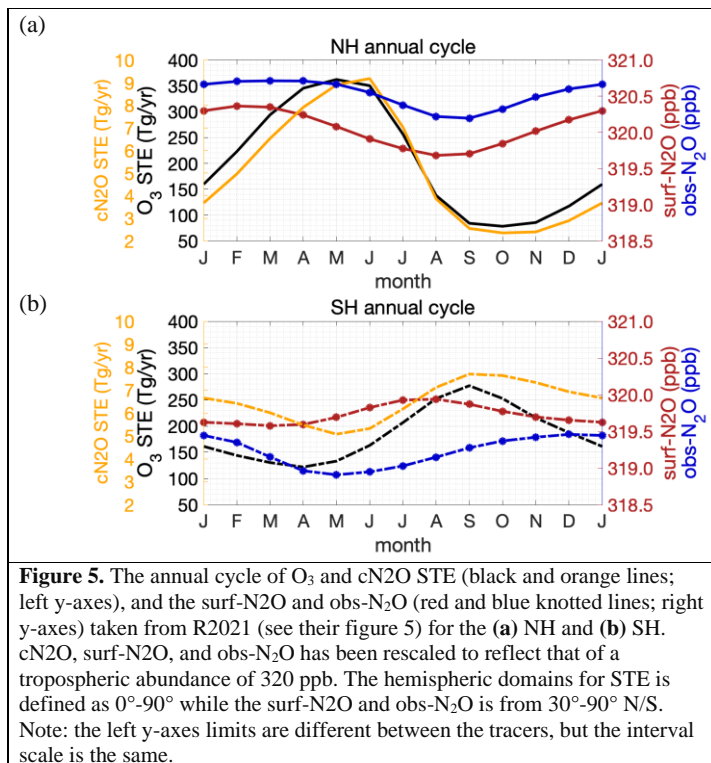
Figure 5. The annual cycle of O_3 and cN2O STE (black and orange lines; left y-axes), and the surf-N2O and obs-N2O (red and blue knotted lines; right y-axes) taken from R2021 (see their figure 5) for the **(a)** NH and **(b)** SH. cN2O, surf-N2O, and obs-N2O has been rescaled to reflect that of a tropospheric abundance of 320 ppb. The hemispheric domains for STE is defined as 0°-90° while the surf-N2O and obs-N2O is from 30°-90° N/S. Note: the left y-axes limits are different between the tracers, but the interval scale is the same.

384
385
386   *4.2. QBO cycle*
387
388   The QBO composite of hemispheric mean cN2O STE flux from Figure 4 is compared with the
389   composite of surface abundances (surf-N2O and obs-N2O) in Figure 6. The peak in cN2O flux is
390   broad and flat, but centers on +2 months for the NH and +4 months for the SH. Unlike the
391   annual cycle, the QBO cycle in STE flux is almost in phase in both hemispheres, with the NH
392   preceding the SH. This phasing of the QBO cycle in surface N_2O was seen with the three
393   models in R2021. In both hemispheres, the modeled surf-N2O peaks before the rise in cN2O
394   and then decreases through most of the period with elevated cN2O flux as expected. The
395   amplitude of the QBO STE flux is smaller in the NH than SH by about half, and the amplitude of
396   surf-N2O is likewise smaller. The ratio of the amplitudes of surf-N2O to cN2O STE flux is
397   similar in both hemispheres (~ 0.4 ppb per Tg/yr), which is encouraging. This ratio is larger than
398   the corresponding one from the annual cycles (~ 0.1 ppb per Tg/yr) because the length of the
399   QBO cycle leads to longer accumulation of N_2O-depleted air from the cN2O flux.
400
401   In the SH, where the QBO cycle in cN2O flux has a large amplitude, the modeled surf-N2O
402   matches obs-N2O in amplitude and phase as reported in R2021. In the NH, the comparison of

surf-N2O with obs-N$_2$O is not so good: obs-N$_2$O has a much smaller amplitude and a different
phase. This QBO cycle pattern is similar, but reversed, to that of the annual cycle and can be
understood in the same way. The NH QBO cycle has relatively small amplitude and thus the
interference with the large-amplitude annual cycle adds noise, obscuring the QBO cycle. In the
SH it is the opposite, with its weak annual cycle, the SH QBO cycle is clear. The modeled cN2O
fluxes enable us to understand the large-scale variability of the observations.

Thus, for both annual and QBO fluctuations, when the variation in STE flux is dominated by
either cycle, the surface variations are clearly seen and modeled for that cycle. This further
supports the findings in R2021 and other studies, that hemispheric surface N$_2$O variability is
driven by stratospheric loss on annual (NH) and QBO (SH) cycles, and it is clearly tied to the
STE flux. Given the connection between O$_3$ and cN2O STE, this relational metric can be used to
constrain the O$_3$ STE for a model ensemble.

Figure 6. **(a)** NH and **(b)** SH QBO composites of cN2O STE flux
(Tg/yr; orange lines, left axis, Fig. 4), and surf-N2O and obs-N$_2$O
(ppb; red and blue knotted lines, right axes, see Fig. 3 of R2021).
Results are shown for years 2001-2016 (6 QBO phase transitions), see
Fig. 4. The surf-N2O data is from UCI CTM, and obs-N$_2$O are taken
from NOAA ESRL, see text.
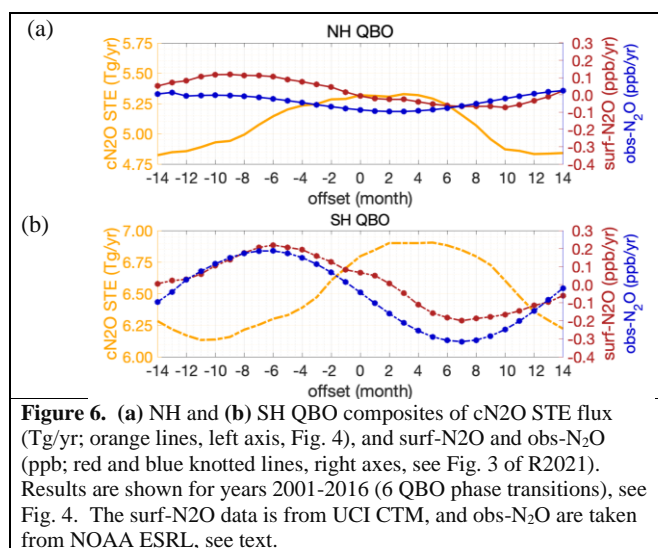
5. Lowermost stratosphere

If we accept that matching the observed annual and QBO cycles in surface N$_2$O constrains the
modeled STE cN2O flux, then how can we use that to also constrain the modeled STE O$_3$ flux?
All evidence, theoretical, observational, and modeled, shows that the STE flux is simultaneous
for all species (e.g., Figure 1) and in proportion to their relative abundances (i.e., tracer:tracer
slopes) in the lowermost stratosphere, defined roughly as the region 100-200 hPa in each
hemisphere outside the tropics (Plumb and Ko, 1992).

5.1. The O$_3$:N$_2$O slopes and STE fluxes

429 We can test the Plumb and Ko hypothesis in our model framework by comparing the relative
430 STE fluxes for O_3, cN2O and cF11 with the modeled tracer-tracer slopes in the lowermost
431 stratosphere. These slopes can then be tested using SCISAT-1 ACE-FTS (Scientific Satellite-1
432 Atmospheric Chemistry Experiment-Fourier Transform Spectrometer) measurements of O_3 and
433 N_2O in the lowermost stratosphere to establish the ratio of the two STE fluxes. The ACE-FTS
434 O_3:N_2O slopes were used for model transport and chemistry evaluation (Hegglin and Shepherd,
435 2007) and found to be very sensitive to satellite sampling, except in the lowermost stratosphere.
436
437
438 Figure 7ab shows the N_2O-O_3 slope in each hemisphere taken from the ACE climatology dataset
439 and the UCI CTM. The current ACE dataset (version 3.5) has been curated from measurements
440 made by ACE-FTS from February 2004 to February 2013 (Koo et al., 2017). The SCISAT orbit
441 results in irregular season-latitude coverage, and thus we average the lowermost stratosphere
442 data over a wide range of latitudes centered on the peak STE flux (20°-60° in both hemispheres).
443 For both ACE data and the CTM we keep to the lowermost stratosphere (200-100 hPa) and
444 average over the 4-month peak of STE flux, Feb-May in the NH and Sep-Dec in the SH (see
445 Figure 1). Extending into the upper tropical troposphere at 20° helps define the tropospheric
446 end-point of the slope (low O_3, high N_2O). Our method described here for deriving the slopes
447 from the ACE-FTS data is slightly different from that of Hegglin and Shepherd (2007; e.g., we
448 do not anchor the tropospheric point), and we have the advantage of a longer record.
449
450
451 Based on the long-term mean STE fluxes in the model, we would expect an O_3:N_2O slope of
452 about -24 (ppb/ppb) in the NH and -17 in the SH. The slopes fitted to our modeled grid-cell
453 values of O_3 and N2O in the lowermost stratosphere are remarkably similar: -23.2 (NH) and -
454 17.5 (SH). The ACE data are more scattered but show similar, smaller slopes of -19.4 (NH) and
455 -15.3 (SH). Thus, the NH-SH asymmetry in O_3 versus N_2O STE fluxes is clearly reflected in the
456 tracer-tracer slopes, both modeled and observed. Hegglin and Shepherd (2007) had already
457 identified these NH:SH differences when comparing their model to the ACE-FTS observations
458 (their Fig. 13cd), but implications for STE fluxes were not brought forward.
459
460 In the modeled SH (Figure 7b), one can see strings of points that are samples along neighboring
461 cells and reflect a linear mixing line between two different end points, one of which has
462 experienced extensive O_3 depletion (i.e., the Antarctic O_3 hole). We know that there is some
463 chemical loss of O_3 in the NH lowermost polar stratosphere during very cold winters (Manney et
464 al., 2011; Isaksen et al., 2012), but it is not extensive enough to systematically affect the O_3:N_2O
465 slope over the mid-latitude lowermost stratosphere in either the ACE observations or the CTM
466 simulations.
467
468
469
470
471
472
473
474

Figure 7. O_3 versus N_2O (x-axis) scatter plots from **(a)** SCISAT ACE-FTS and **(b)** the UCI CTM. ACE-FTS data is from monthly climatologies for the period Feb 2004 to Feb 2013 restricted to 200-100 hPa, latitudes about 20°-60°, and months Feb-May (NH, red) or Sep-Dec (SH, blue). The linear-fit lines (ppb/ppb, values in legend) are restricted to larger N_2O values (>280 ppb) to more accurately represent the STE fluxes, see Olsen et al. (2001).

5.2. IAV of the Antarctic ozone hole and the SH STE O_3 flux

The Antarctic ozone hole appears to be the source of the NH-SH asymmetry in the STE fluxes of O_3 versus N_2O. It is known that the massive chemical depletion of O_3 inside the Antarctic vortex between about 13 and 23 km altitude creates an air mass with lower $O_3:N_2O$ ratios than usually found in the mid-latitude lowermost stratosphere. When the vortex breaks up, nominally in late November, much of this O_3-depleted air can mix along isentropes into the mid-latitude lowermost stratosphere, changing the $O_3:N_2O$ ratios and reducing the SH STE O_3 flux.

We have additional information on the SH O_3 STE flux from the year-to-year variations in the size of the ozone hole. The best measure of the scale of Antarctic ozone depletion is the October mean ozone column (DU) averaged from the pole to 63°S equivalent latitude (see Fig. 4-5 of WMO, 2018). When we compare the CTM with the observations (Figure 8), we find remarkable verisimilitude in the model: the root-mean-squared difference is 9 DU out of a standard deviation of 29 DU and the correlation coefficient is 0.96. Thus, we have confidence that we are simulating the correct IAV of the ozone hole. Next, we plot the modeled O_3 STE flux (summed over the 12 months following the peak ozone hole, November-October) with the modeled October ozone column and find a fairly linear relationship. If we estimate the STE O_3 flux

501   before the O_3 hole, when the mean October O_3 column was about 307 DU, then our O_3 flux
502   increases to 209 Tg/yr (see Figure 8, red marker), eliminating the hemispheric asymmetry in O_3
503   STE flux.
504
505   The annual deficit in SH STE O_3 flux brought on by the Antarctic ozone hole ranges from about
506   5 to 55 Tg/yr and with a central value of 30 Tg/yr or 14% of the total. Using the decadal trends
507   1965-2000 from Hegglin and Shepherd (2009), this deficit is 8%; and from Meul et al. (2018),
508   5%. Since both of these models calculate a much larger SH flux (~300 Tg/yr), we estimate their
509   absolute change in O_3 flux to be 24 and 15 Tg/yr, respectively. Because the ozone hole
510   effectively removes a fixed, rather than proportional, amount of ozone that presumably is
511   mapped onto the STE flux the following year, we believe the absolute change is the best
512   measure. Thus the three models estimate the ozone hole causes a deficit in the SH O_3 STE flux
513   in the range of 15-30 Tg/yr. The UCI CTM's ability to match the observed IAV of the ozone
514   hole, and to match that linearly with the deficit in STE flux provides support for the upper end of
515   the range. Note that the difference in O_3:N_2O slopes between NH and SH in Figure 7 is about 5.
516   If we attribute that solely to the ozone hole and split the flux of N_2O-depleted air evenly between
517   hemispheres, then the ozone-hole-driven O_3 STE flux difference is about 55 Tg/yr, about twice
518   that derived from the variability in our model. This difference in estimated flux indicates that
519   even without chlorine-driven ozone depletion, the O_3:N_2O slopes may be inherently different
520   simply because of the strong descent inside the wintertime Antarctic vortex. This can be readily
521   investigated with further model studies.
522
523   We looked for any relationship between ozone hole IAV and the STE fluxes of cN2O or cF11
524   and found mostly a scatter plot with no clear relationship. Given the analysis above, we expect
525   that much of the scatter is related to QBO cycles.
526
527
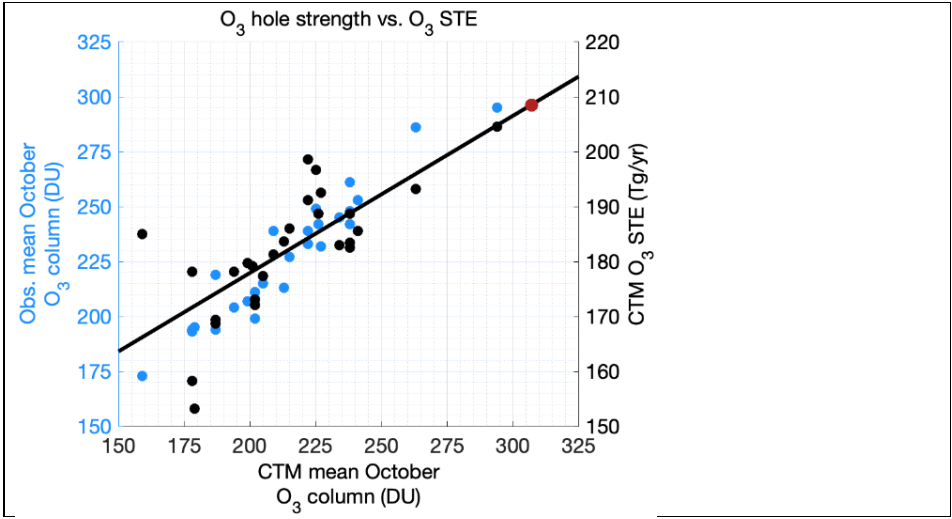
Figure 8. Interannual variability of the observed Antarctic ozone hole from 1990 to 2017 (blue dots; left y-axis) versus the CTM modeled ozone hole (x-axis); plus the CTM modeled SH STE O_3 flux (black dots; right y-axis) versus the modeled ozone hole (x-axis). The ozone hole is measured by the total ozone column (DU) averaged daily over October poleward of 63°S in equivalent latitude (see Figure 4.5 of WMO 2018). The SH STE O_3 flux (Tg/yr) is centered on May 1 of the following year (i.e., the 12 months following the nominal breakup of the ozone hole). The black line is a simple regression fit of the modeled STE to the modeled ozone hole (black dots), and the red dot is our estimate of pre-ozone-hole SH STE O_3 flux based on the observed 1979-82 O_3 column.

528
529
530 *5.3 Other model-measurement metrics related to STE*
531
532 What else might affect O_3 STE? Stratospheric column O_3 (DU) varies on annual and QBO
533 timescales. These changes in O_3 overhead can have a direct influence on O_3 transport to the
534 troposphere, but the link requires further analysis. Tang et al. (2021) showed the UCI CTM is
535 able to capture the observed annual cycle of stratospheric O_3 column as extracted from total
536 column using the Ziemke et al. (2019) method. QBO modulation of stratospheric column O_3 has
537 not been fully investigated since Tung and Yang (1994b). Yet, the fluctuations in mass over the
538 annual cycle are comparable to the corresponding variability in O_3 STE flux (1 DU = 10.9 Tg)
539 and likely connected (Figure 9).
540
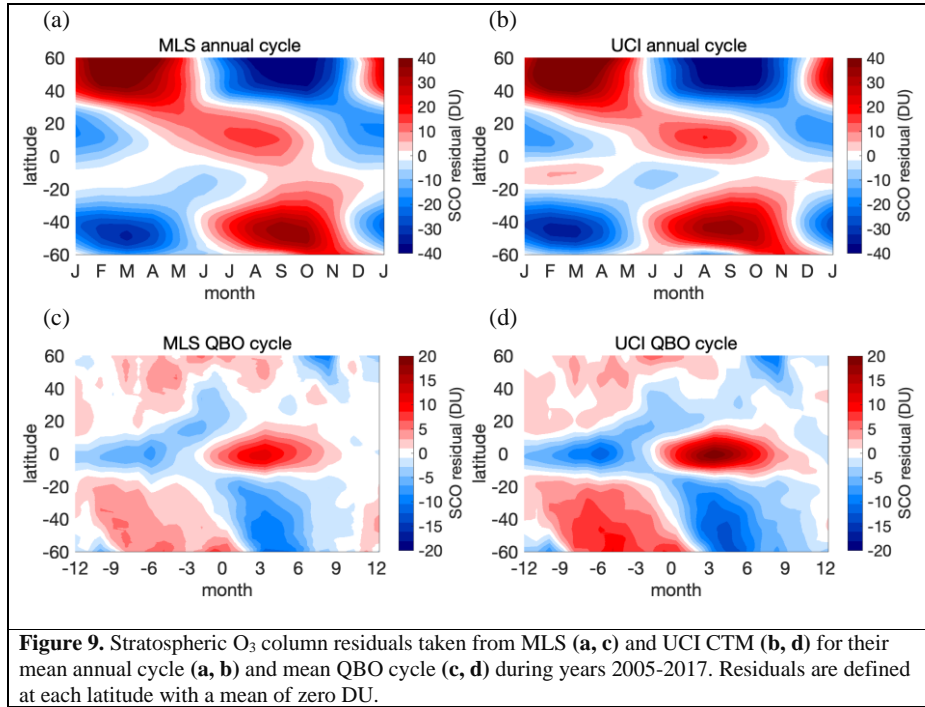
Figure 9. Stratospheric O_3 column residuals taken from MLS **(a, c)** and UCI CTM **(b, d)** for their mean annual cycle **(a, b)** and mean QBO cycle **(c, d)** during years 2005-2017. Residuals are defined at each latitude with a mean of zero DU.

541

542
543 **6. Conclusions**
544
545 This work examines how closely O_3 STE is linked to STE fluxes of other trace gases. By
546 including our complementary N_2O and F11 tracers, we can follow stratospheric loss of these
547 gases along with stratospheric O_3 across the tropopause. The magnitudes of the fluxes are
548 proportional to their abundances in the lower stratosphere as expected (Plumb and Ko, 1992),
549 and their variability is highly correlated with one another, indicating that they are entering the
550 troposphere simultaneously. Even the distinct QBO pattern of STE fluxes is consistent across
551 O_3, N_2O and F11. We further constrain the N_2O transport pathway by linking STE of depleted-
552 N_2O air with surface fluctuations of N_2O abundance. The surface response in modeled N_2O
553 matches well with the observed surface variability in the SH, indicating that surface variability is
554 driven largely by STE flux.
555
556 *Consistency of STE O_3 flux*. As summarized here, there are a number of model diagnostics and
557 observational constraints that provide a reality check on the consistency of the modeled O_3 STE
558 flux. In Table 1, we examine these for our model and also for the CMAM model (Hegglin and
559 Shepherd, 2007, 2009) because it is one of the few with enough published results. For UCI we
560 calculate NH:SH fluxes of O_3 (208:182 Tg-O_3/yr) and N_2O (5.1:6.4 Tg-N/yr). Thus the mole
561 fraction slopes in the lowermost stratosphere should be -23.8 (NH) and -16.6 (SH). Our model
562 O_3:N_2O slopes are -23.2 (NH) and -17.5 (SH). Given the seasonal variability and scatter in the
563 correlation plots (Figure 7), we count this as consistent. For CMAM, the modeled O_3:N_2O
564 slopes, -23±21 (NH) and -18±3 (SH) are similar to ours and also to the ACE-FTS observations
565 as analyzed by Hegglin and Shepherd (2007), -22 22±4 (NH) and -14±35 (SH), or by us, -19
566 (NH) and -15 (SH). CMAM does not report the implied STE N_2O fluxes derived from their
567 photochemical loss of N_2O, but their model seems to match observations of N_2O in the middle
568 stratosphere, and so we assume that the Aura-MLS- derived N_2O fluxes are a close estimate
569 (12.9 Tg-N/yr). Note we are using Aura-MLS N_2O values here to calculate the photochemical
570 loss, which occurs in. the middle to upper stratosphere (see R2021 for methodology). Just using
571 the CMAM global numbers for O_3 STE flux, we calculate the O_3:N_2O slope in the lowermost
572 stratosphere should average to -30. We conclude that their diagnosis of the STE O_3 flux, 655
573 Tg/yr, is inconsistent with the circulation that generated the O_3:N_2O slopes and is 50% too large.
574 We do not view this as a critical assessment of CMAM since it involves us combining
575 diagnostics from two separate publications and possibly different model simulations, but it is an
576 example of how we might expect future studies of the STE O_3 flux to self-evaluate.
577
578 *Uncertainty Quantification in STE O_3 flux*. Deriving a best estimate and uncertainty from this
579 work involves expert judgment. Changes in meteorological data used by the UCI CTM (IFS
580 Cycles 29r1, 36r1, and 38r1, all at 60-layer 1.1° resolution, see Table 1) give a standard
581 deviation in STE of 13% (only 3 values). If we use observations to derive a value as in Murphy
582 and Fahey (1994), we must expand our dimensions to the uncertainty in the NH:SH split of N_2O
583 flux to calculate each hemisphere's O_3 flux. The factors are: (1) total STE N_2O flux is 12.9 Tg-
584 N/yr from the MLS data and we assign a ±10% one-sigma uncertainty; (2) the NH:SH split of
585 the N_2O flux is 44:56 in our current model, was not diagnosed for previous ones, and so we
586 assume a value of 50:50 that ranges from 40:60 to 60:40; (3) analysis of the ACE-FTS
587 observations (ours and Hegglin and Shepherd, 2007) gives O_3:N_2O slopes of about -21 (NH) and

588 -15 (SH) to which we assign a one-sigma uncertainty of ±3. Propagating these as root-mean
589 square errors, we find a ±15% uncertainty in the global value, 400 ± 60 Tg/yr. Uncertainty in the
590 hemispheric values is more difficult to assess, and from a range of model results shown in Table
591 1, we can only estimate that the NH:SH ratio is between 60:40 and 50:50, a range that bounds
592 our and CMAM results plus 2%. Note that this estimate is for current conditions with a regularly
593 occurring Antarctic ozone hole. We believe the low 50:50 ratio is plausible because we have
594 shown that our large SH STE N_2O flux is consistent with the surface QBO variability in N_2O.
595 For pre-1980, and for when the ozone hole recovers later this century, we anticipate that the SH
596 $O_3:N_2O$ slope will revert to -18 to -21, and the total STE O_3 flux to 430-460 Tg/yr. This
597 simplistic estimate is based on a fixed atmospheric circulation.
598
599 A major surprise from our model is that the STE flux of O_3 is predominantly NH biased
600 currently, only because of the Antarctic ozone hole. Prior to 1980, and after 2060, it would/will
601 be symmetric between the hemispheres. Our model calculates slightly greater STE fluxes for
602 trace gases like N_2O or F11 in the SH, which is counter to prevailing theory that the wave-driven
603 fluxes force relatively greater STE in the NH. This difference cannot be directly tested with
604 observations of trace gases, but a range of N_2O hemispheric observations are well modeled and
605 support this premise. More extensive work with multi-model ensembles that include both
606 chemical and dynamical diagnostics in the stratosphere would be needed to overturn the
607 established theory. Our work reemphasizes the importance of trace-gas correlations in the
608 lowermost stratosphere as a key observational metric for climate models that may be able to
609 constrain total STE fluxes. The tracer slopes may go beyond just relative STE fluxes because we
610 have other measurements from the upper stratosphere to the surface that constrain, for example,
611 the absolute flux of N_2O better than we first did using just the modeled lifetime.
612
613 In Table 2, we gather a set of observation-based model metrics that relate to STE fluxes and will
614 help the community build more robust models to better derive the STE flux of O_3.
615

Table 1. Summary of key results for the STE flux of O_3 and N_2O presented here (bold)				
	NH	SH	Global	notes
STE O_3 flux (TgO_3/yr)	**208**	**182**	**390**	IFS Cy38r1, yrs 1990-2017 (this paper; Ruiz et al., 2021)
	239	198	437	IFS Cy36r1, yrs 2000-2007 (Hsu & Prather, 2014)
	301	233	534	IFS Cy29r1, yrs 2000-2006 (Hsu & Prather, 2014)
	383	272	655	CMAM, yrs 1995-2005 (Hegglin & Shepherd, 2009)
STE N_2O flux (TgN/yr)	**5.1**	**6.4**	**11.5**	yrs 1990-2017, scaled to 320 ppb
			12.9	using MLS lifetime of 119 yr and 320 ppb
LMS $O_3:N_2O$ slope*	**-23.2**	**-17.5**		UCI model
	-19.4	**-15.3**		ACE-FTS observations
	-23±2.0	-18±37.5		CMAM model, Fig 13 of (Hegglin & Shepherd, 2007)
	-22±4.0	-14±35.0		ACE-FTS observations, ibid
			-20.0	(Murphy & Fahey, 1994)
			-22.0	(McLinden et al., 2000)

STE flux O$_3$:N$_2$O (mole/mole)	**-23.8**	**-16.6**		UCI model, calculated from entries above
			-29.6	CMAM (Hegglin & Shepherd, 2009), using MLS N$_2$O lifetime
Best Estimate STE O$_3$ flux (Tg/yr)	**60% to 50%**	**40% to 50%**	**400 ± 60**	current Antarctic ozone hole conditions, see text
* LMS = lowermost stratosphere only. For UCI model, months are selected for highest STE (FMAM in NH, SOND in SH, Fig. 1). For CMAM, the monthly ranges~~annual averages~~ from their Fig. 13cd are estimated. Where no reference is given, the source is this paper.				

616
617

Table 2. Metrics from Measurements or Constrained Values for CCMs related to Stratosphere-Troposphere Exchange

Name	Metric	Measured values	Model requirements	Example figure
N$_2$O loss	Annual and QBO cycles of global mean stratospheric N$_2$O loss	Monthly N$_2$O loss calculated from MLS profiles (2005-present)	Stratospheric chemistry for N$_2$O as tracer; a QBO cycle; monthly mean diagnostics	Fig. 4 (Prather et al., 2015); Fig. 2 (Ruiz et al., 2021); Fig. 3 (this paper)
STE slopes	Matching O$_3$:N$_2$O slopes in lowermost stratosphere	ACE FTS profiles (2004-2013)	Stratospheric O$_3$ and N$_2$O calculation, possibly also CFCs; monthly snapshots	Fig. 7 (this paper)
Strat O$_3$ column	Annual and QBO composite cycles of stratospheric O$_3$ column	Monthly zonal mean stratospheric O$_3$ column from Ziemke et al., 2019 (2005-present)	Stratospheric O$_3$ chemistry; a QBO cycle; monthly mean diagnostics; separate strat & trop O$_3$ columns	Fig. 9 (this paper)
N$_2$O loss at surface	Annual and QBO composite cycles of surface N$_2$O solely from stratospheric loss	NOAA surface N$_2$O observations	Stratospheric N$_2$O chemistry; N2OX as a tracer; monthly mean diagnostics	Fig. 3 (Ruiz et al., 2021); Fig. 5 (this paper)
		Constrained (modeled) values		
STE flux of O$_3$		Monthly, latitude or hemispheric resolved, net O$_3$ flux	Run O3strat as a tracer; diagnose monthly flux into troposphere, at tropopause or through trop- loss of O3strat	Fig. 1 & 2 (this paper)
STE flux of N$_2$O depleted air (also CFC-11)		Monthly, latitude or hemispheric resolved, STE flux of N$_2$O (CFC-11)	Run cN2O (cF11) as a tracer; diagnose monthly flux into troposphere	Fig. 1 & 2 (this paper);
SH O$_3$ hole and flux		Change in SH O$_3$ STE flux with size of ozone hole; observed IAV of O$_3$ hole	IAV of ozone hole; daily total O$_3$ column (lat, long); monthly SH O$_3$ STE flux	Fig 7 (this paper)
Notes: Constrained values are model-only derived quantities that can be diagnosed from CCMs or CTMs.				

618
619
620
621

622
623
624
625
626
627
628
629
630
631
632
633
634 **Author Contributions:**
635
636 DJR and MJP designed and carried out the study and prepared the manuscript for publication.
637
638
639 **Competing interests:**
640
641 The authors declare that they have no conflict of interest.
642
643
644 **Acknowledgments:**
645

646 Research at UCI was supported by grants from the National Aeronautics and Space
647 Administration's Modeling, Analysis and Prediction Program (award NNX13AL12G), and
648 Atmospheric Chemistry Modeling and Analysis Program (80NSSC20K1237, NNX15AE35G),
649 and the National Science Foundation (NRT-1633631). We gratefully acknowledge the work of
650 the MLS team in producing the Level 3 data sets that enabled our MLS-related analyses. Work at
651 the Jet Propulsion Laboratory, California Institute of Technology, was performed under contract
652 with the National Aeronautics and Space Administration. We thank the ACE-FTS team for
653 making the climatology data used here available for our analyses. The Atmospheric Chemistry
654 Experiment (ACE), also known as SCISAT, is a Canadian-led mission mainly supported by the
655 Canadian Space Agency. We also acknowledge Ed Dlugokencky for providing the surface N_2O
656 data that was used here to produce an observation-based reference with which to compare our
657 simulated results. The data used to produce the figures and tables in this work are accessible via
658 the DRYAD repository with DOI https://doi.org/10.7280/D1JX0K

659
660
661

662

663

664

665

666

667

668

669

670

671

672

673

References:

Appenzeller, C., Holton, J. R., and Rosenlof, K. H.: Seasonal variation of mass transport across the tropopause, J Geophys Res-Atmos, 101, 15071-15078, doi:10.1029/96JD00821, 1996.

Baldwin, M. P., Gray, L. J., Dunkerton, T. J., Hamilton, K., Haynes, P. H., Randel, W. J., Holton, J. R., Alexander, M. J., Hirota, I., Horinouchi, T., Jones, D. B. A., Kinnersley, J. S., Marquardt, C., Sato, K., and Takahashi, M.: The quasi-biennial oscillation, Reviews of Geophysics, 39, 179-229, 2001.

Butterbach-Bahl, K., Baggs, E. M., Dannenmann, M., Kiese, R., and Zechmeister-Boltenstern, S.: Nitrous oxide emissions from soils: how well do we understand the processes and their controls?, Philos T R Soc B, 368, 10.1098/rstb.2013.0122, 2013.

Dlugokencky, E. J., Crotwell, A. M., Mund, J. W., Crotwell, M. J., and Thoning, K. W.: Atmospheric Nitrous Oxide Dry Air Mole Fractions from the NOAA ESRL Carbon Cycle Cooperative Global Air Sampling Network, 1997-2018, Version: 2019-07, 10.15138/53g1-x417, 2019.

Gettelman, A., Holton, J. R., and Rosenlof, K. H.: Mass fluxes of O-3, CH4, N2O and CF2Cl2 in the lower stratosphere calculated from observational data, J Geophys Res-Atmos, 102, 19149-19159, Doi 10.1029/97jd01014, 1997.

Griffiths, P. T., Murray, L. T., Zeng, G., Shin, Y. M., Abraham, N. L., Archibald, A. T., Deushi, M., Emmons, L. K., Galbally, I. E., Hassler, B., Horowitz, L. W., Keeble, J., Liu, J., Moeini, O., Naik, V., O'Connor, F. M., Oshima, N., Tarasick, D., Tilmes, S., Turnock, S. T., Wild, O., Young, P. J., and Zanis, P.: Tropospheric ozone in CMIP6 simulations, Atmos Chem Phys, 21, 4187-4218, 10.5194/acp-21-4187-2021, 2021.

Hamilton, K., and Fan, S. M.: Effects of the stratospheric quasi-biennial oscillation on long-lived greenhouse gases in the troposphere, J Geophys Res-Atmos, 105, 20581-20587, 10.1029/2000jd900331, 2000.

Hegglin, M. I., and Shepherd, T. G.: Large climate-induced changes in ultraviolet index and stratosphere-to-troposphere ozone flux, Nature Geoscience, 2, 687-691, Doi 10.1038/Ngeo604, 2009.

Hegglin, M. I., and Shepherd, T. G.: O3-N2O correlations from the Atmospheric Chemistry Experiment: Revisiting a diagnostic of transport and chemistry in the stratosphere, J Geophys Res-Atmos, 112, Artn D19301, 10.1029/2006jd008281, 2007.

706 Hess, P., Kinnison, D., and Tang, Q.: Ensemble simulations of the role of the stratosphere in the
707   attribution of northern extratropical tropospheric ozone variability, Atmos Chem Phys, 15,
708   2341-2365, 10.5194/acp-15-2341-2015, 2015.
709 Hirsch, A. I., Michalak, A. M., Bruhwiler, L. M., Peters, W., Dlugokencky, E. J., and Tans, P. P.:
710   Inverse modeling estimates of the global nitrous oxide surface flux from 1998-2001, Global
711   Biogeochem Cy, 20, Artn Gb1008, 10.1029/2004gb002443, 2006.
712 Holton, J. R., Haynes, P. H., Mcintyre, M. E., Douglass, A. R., Rood, R. B., and Pfister, L.:
713   Stratosphere-Troposphere Exchange, Reviews of Geophysics, 33, 403-439, 1995.
714 Holton, J. R.: On the Global Exchange of Mass between the Stratosphere and Troposphere, J
715   Atmos Sci, 47, 392-395, Doi 10.1175/1520-0469(1990)047<0392:Otgeom>2.0.Co;2, 1990.
716 Hsu, J. N., and Prather, M. J.: Is the residual vertical velocity a good proxy for stratosphere-
717   troposphere exchange of ozone?, Geophys Res Lett, 41, 9024-9032,
718   10.1002/2014GL061994, 2014.
719 Hsu, J., and Prather, M. J.: Global long-lived chemical modes excited in a 3-D chemistry
720   transport model: Stratospheric N_2O, NOy, O_3 and CH_4 chemistry, Geophys Res Lett, 37,
721   L07805, Artn L07805, 10.1029/2009gl042243, 2010.
722 Hsu, J., and Prather, M. J.: Stratospheric variability and tropospheric ozone, J Geophys Res-
723   Atmos, 114, Artn D06102, 10.1029/2008jd010942, 2009.
724 Hsu, J., Prather, M. J., and Wild, O.: Diagnosing the stratosphere-to-troposphere flux of ozone in
725   a chemistry transport model, J Geophys Res-Atmos, 110, Artn D19305,
726   10.1029/2005jd006045, 2005.
727 Isaksen, I. S. A., Zerefos, C., Wang, W. C., Balis, D., Eleftheratos, K., Rognerud, B., Stordal, F.,
728   Berntsen, T. K., LaCasce, J. H., Sovde, O. A., Olivie, D., Orsolini, Y. J., Zyrichidou, I.,
729   Prather, M., and Tuinder, O. N. E.: Attribution of the Arctic ozone column deficit in March
730   2011, Geophys Res Lett, 39, Artn L24810, 10.1029/2012gl053876, 2012.
731 Kinnersley, J. S., and Tung, K. K.: Mechanisms for the extratropical QBO in circulation and
732   ozone, J Atmos Sci, 56, 1942-1962, Doi 10.1175/1520-
733   0469(1999)056<1942:Mfteqi>2.0.Co;2, 1999.
734 Koo, J. H., Walker, K. A., Jones, A., Sheese, P. E., Boone, C. D., Bernath, P. F., & Manney, G.
735   L.: Global climatology based on the ACE-FTS version 3.5 dataset: Addition of mesospheric
736   levels and carbon-containing species in the UTLS. Journal of Quantitative Spectroscopy and
737   Radiative Transfer, 186, 52–62, 10.1016/j.jqsrt.2016.07.003, 2017.
738 Liang, Y. X., Gillett, N. P., and Monahan, A. H.: Climate Model Projections of 21st Century
739   Global Warming Constrained Using the Observed Warming Trend, Geophys Res Lett, 47,
740   ARTN e2019GL086757, 10.1029/2019GL086757, 2020.
741 Liu, H. Y., Considine, D. B., Horowitz, L. W., Crawford, J. H., Rodriguez, J. M., Strahan, S. E.,
742   Damon, M. R., Steenrod, S. D., Xu, X. J., Kouatchou, J., Carouge, C., and Yantosca, R. M.:
743   Using beryllium-7 to assess cross-tropopause transport in global models, Atmos Chem Phys,
744   16, 4641-4659, 10.5194/acp-16-4641-2016, 2016.
745 Manney, G. L., Santee, M. L., Rex, M., Livesey, N. J., Pitts, M. C., Veefkind, P., Nash, E. R.,
746   Wohltmann, I., Lehmann, R., Froidevaux, L., Poole, L. R., Schoeberl, M. R., Haffner, D. P.,
747   Davies, J., Dorokhov, V., Gernandt, H., Johnson, B., Kivi, R., Kyro, E., Larsen, N., Levelt,
748   P. F., Makshtas, A., McElroy, C. T., Nakajima, H., Parrondo, M. C., Tarasick, D. W., von
749   der Gathen, P., Walker, K. A., and Zinoviev, N. S.: Unprecedented Arctic ozone loss in
750   2011, Nature, 478, 469-U465, 10.1038/nature10556, 2011.

751 McLinden, C. A., Olsen, S. C., Hannegan, B., Wild, O., Prather, M. J., and Sundet, J.:
752   Stratospheric ozone in 3-D models: A simple chemistry and the cross-tropopause flux, J
753   Geophys Res-Atmos, 105, 14653-14665, 10.1029/2000JD900124, 2000.
754 Meul, S., Langematz, U., Kroger, P., Oberlander-Hayn, S., and Jockel, P.: Future changes in the
755   stratosphere-to-troposphere ozone mass flux and the contribution from climate change and
756   ozone recovery, Atmos Chem Phys, 18, 7721-7738, 10.5194/acp-18-7721-2018, 2018.
757 Montzka, S. A., Dutton, G. S., Yu, P. F., Ray, E., Portmann, R. W., Daniel, J. S., Kuijpers, L.,
758   Hall, B. D., Mondeel, D., Siso, C., Nance, D., Rigby, M., Manning, A. J., Hu, L., Moore, F.,
759   Miller, B. R., and Elkins, J. W.: An unexpected and persistent increase in global emissions
760   of ozone-depleting CFC-11, Nature, 557, 413-416, 10.1038/s41586-018-0106-2, 2018.
761 Murphy, D. M., and Fahey, D. W.: An estimate of the flux of stratospheric reactive nitrogen and
762   ozone into the troposphere, Journal of Geophysical Research, 99, 5325-5332, 1994.
763 Nevison, C. D., Kinnison, D. E., and Weiss, R. F.: Stratospheric influences on the tropospheric
764   seasonal cycles of nitrous oxide and chlorofluorocarbons, Geophys Res Lett, 31, Artn
765   L20103, 10.1029/2004gl020398, 2004.
766 Nevison, C. D., Mahowald, N. M., Weiss, R. F., and Prinn, R. G.: Interannual and seasonal
767   variability in atmospheric N2O, Global Biogeochem Cy, 21, Artn Gb3017,
768   10.1029/2006gb002755, 2007.
769 Newman, P.: The quasi-biennial oscillation (QBO), NASA, Goddard Space Flight Center,
770   https://acd-ext.gsfc.nasa.gov/Data_services/met/qbo/qbo.html, retrieved on 3 Mar 2020.
771 Olsen, M. A., Manney, G. L., and Liu, J. H.: The ENSO and QBO Impact on Ozone Variability
772   and Stratosphere-Troposphere Exchange Relative to the Subtropical Jets, J Geophys Res-
773   Atmos, 124, 7379-7392, 10.1029/2019JD030435, 2019.
774 Olsen, M. A., Schoeberl, M. R., and Douglass, A. R.: Stratosphere-troposphere exchange of mass
775   and ozone, J Geophys Res-Atmos, 109, Artn D24114, 10.1029/2004jd005186, 2004.
776 Olsen, S. C., McLinden, C. A., and Prather, M. J.: Stratospheric N2O-NOy system: testing
777   uncertainties in a three-dimensional framework, J. Geophys. Res., 106, 28771-28784, 2001.
778 Plumb, R. A., and Ko, M. K. W.: Interrelationships between Mixing Ratios of Long Lived
779   Stratospheric Constituents, J Geophys Res-Atmos, 97, 10145-10156, 1992.
780 Prather, M. J., Hsu, J., DeLuca, N. M., Jackman, C. H., Oman, L. D., Douglass, A. R., Fleming,
781   E. L., Strahan, S. E., Steenrod, S. D., Sovde, O. A., Isaksen, I. S. A., Froidevaux, L., and
782   Funke, B.: Measuring and modeling the lifetime of nitrous oxide including its variability, J
783   Geophys Res-Atmos, 120, 5693-5705, 10.1002/2015JD023267, 2015.
784 Prather, M. J., Zhu, X., Tang, Q., Hsu, J., and Neu, J. L.: An atmospheric chemist in search of
785   the tropopause, J. Geophys. Res., 116, D04306, 10.1029/2010jd014939, 2011.
786 Ray, E. A., Portmann, R. W., Yu, P. F., Daniel, J., Montzka, S. A., Dutton, G. S., Hall, B. D.,
787   Moore, F. L., and Rosenlof, K. H.: The influence of the stratospheric Quasi-Biennial
788   Oscillation on trace gas levels at the Earth's surface, Nat Geosci, 13, 22-24, 10.1038/s41561-
789   019-0507-3, 2020.
790 Ruiz, D. J., Prather, M. J., Strahan, S. E., Thompson, R. L., Froidevaux, L., and Steenrod, S. D.:
791   How Atmospheric Chemistry and Transport Drive Surface Variability of N2O and CFC-11,
792   J Geophys Res-Atmos, 126, ARTN e2020JD033979, 10.1029/2020JD033979, 2021.
793 Stohl, A., Bonasoni, P., Cristofanelli, P., Collins, W., Feichter, J., Frank, A., Forster, C.,
794   Gerasopoulos, E., Gaggeler, H., James, P., Kentarchos, T., Kromp-Kolb, H., Kruger, B.,
795   Land, C., Meloen, J., Papayannis, A., Priller, A., Seibert, P., Sprenger, M., Roelofs, G. J.,
796   Scheel, H. E., Schnabel, C., Siegmund, P., Tobler, L., Trickl, T., Wernli, H., Wirth, V.,

797   Zanis, P., and Zerefos, C.: Stratosphere-troposphere exchange: A review, and what we have
798   learned from STACCATO, J Geophys Res-Atmos, 108, Artn 8516, 10.1029/2002jd002490,
799   2003.
800 Strahan, S. E., Douglass, A. R., Stolarski, R. S., Akiyoshi, H., Bekki, S., Braesicke, P., Butchart,
801   N., Chipperfield, M. P., Cugnet, D., Dhomse, S., Frith, S. M., Gettelman, A., Hardiman, S.
802   C., Kinnison, D. E., Lamarque, J. F., Mancini, E., Marchand, M., Michou, M., Morgenstern,
803   O., Nakamura, T., Olivie, D., Pawson, S., Pitari, G., Plummer, D. A., Pyle, J. A., Scinocca,
804   J. F., Shepherd, T. G., Shibata, K., Smale, D., Teyssedre, H., Tian, W., and Yamashita, Y.:
805   Using transport diagnostics to understand chemistry climate model ozone simulations, J
806   Geophys Res-Atmos, 116, Artn D17302, 10.1029/2010jd015360, 2011.
807 Tang, Q., and Prather, M. J.: Correlating tropospheric column ozone with tropopause folds: the
808   Aura-OMI satellite data, Atmos Chem Phys, 10, 9681-9688, 10.5194/acp-10-9681-2010,
809   2010.
810 Tang, Q., Hess, P. G., Brown-Steiner, B., and Kinnison, D. E.: Tropospheric ozone decrease due
811   to the Mount Pinatubo eruption: Reduced stratospheric influx, Geophys Res Lett, 40, 5553-
812   5558, 10.1002/2013GL056563, 2013.
813 Tang, Q., Prather, M. J., Hsu, J. O., Ruiz, D. J., Cameron, P. J. S., Xie, S. C., and Golaz, J. C.:
814   Evaluation of the interactive stratospheric ozone (O3v2) module in the E3SM version 1
815   Earth system model, Geosci Model Dev, 14, 1219-1236, 10.5194/gmd-14-1219-2021, 2021.
816 Thompson, R. L., Patra, P. K., Ishijima, K., Saikawa, E., Corazza, M., Karstens, U., Wilson, C.,
817   Bergamaschi, P., Dlugokencky, E., Sweeney, C., Prinn, R. G., Weiss, R. F., O'Doherty, S.,
818   Fraser, P. J., Steele, L. P., Krummel, P. B., Saunois, M., Chipperfield, M., and Bousquet, P.:
819   TransCom N2O model inter-comparison - Part 1: Assessing the influence of transport and
820   surface fluxes on tropospheric N2O variability, Atmos Chem Phys, 14, 4349-4368, DOI
821   10.5194/acp-14-4349-2014, 2014.
822 Tian, H. Q., Xu, R. T., Canadell, J. G., Thompson, R. L., Winiwarter, W., Suntharalingam, P.,
823   Davidson, E. A., Ciais, P., Jackson, R. B., Janssens-Maenhout, G., Prather, M. J., Regnier,
824   P., Pan, N. Q., Pan, S. F., Peters, G. P., Shi, H., Tubiello, F. N., Zaehle, S., Zhou, F., Arneth,
825   A., Battaglia, G., Berthet, S., Bopp, L., Bouwman, A. F., Buitenhuis, E. T., Chang, J. F.,
826   Chipperfield, M. P., Dangal, S. R. S., Dlugokencky, E., Elkins, J. W., Eyre, B. D., Fu, B. J.,
827   Hall, B., Ito, A., Joos, F., Krummel, P. B., Landolfi, A., Laruelle, G. G., Lauerwald, R., Li,
828   W., Lienert, S., Maavara, T., MacLeod, M., Millet, D. B., Olin, S., Patra, P. K., Prinn, R. G.,
829   Raymond, P. A., Ruiz, D. J., van der Werf, G. R., Vuichard, N., Wang, J. J., Weiss, R. F.,
830   Wells, K. C., Wilson, C., Yang, J., and Yao, Y. Z.: A comprehensive quantification of
831   global nitrous oxide sources and sinks, Nature, 586, 248-252, 10.1038/s41586-020-2780-0,
832   2020.
833 Tokarska, K. B., Stolpe, M. B., Sippel, S., Fischer, E. M., Smith, C. J., Lehner, F., and Knutti,
834   R.: Past warming trend constrains future warming in CMIP6 models, Sci Adv, 6, ARTN
835   eaaz9549, 10.1126/sciadv.aaz9549, 2020.
836 Tung, K. K., and Yang, H.: Global QBO in Circulation and Ozone 1. Reexamination of
837   Observational Evidence, J Atmos Sci, 51, 2699-2707, Doi 10.1175/1520-
838   0469(1994)051<2699:Gqicao>2.0.Co;2, 1994b.
839 Tung, K. K., and Yang, H.: Global QBO in Circulation and Ozone 2. A Simple Mechanistic
840   Model, J Atmos Sci, 51, 2708-2721, 10.1175/1520-0469(1994)051<2708:Gqicao>2.0.Co;2,
841   1994a.

842 Williams, R. S., Hegglin, M. I., Kerridge, B. J., Jockel, P., Latter, B. G., and Plummer, D. A.:
843   Characterising the seasonal and geographical variability in tropospheric ozone, stratospheric
844   influence and recent changes, Atmos Chem Phys, 19, 3589-3620, 10.5194/acp-19-3589-
845   2019, 2019.
846 WMO: Scientific Assessment of Ozone Depletion: 2018, Global Ozone Research and
847   Monitoring Project—Report No. 58, World Meteorological Organization, Geneva,
848   Switzerland, 588 pp., 2018.
849 Yang, H., Chen, G., Tang, Q., and Hess, P.: Quantifying isentropic stratosphere-troposphere
850   exchange of ozone, J Geophys Res-Atmos, 121, 3372-3387, 10.1002/2015JD024180, 2016.
851 Young, P. J., Archibald, A. T., Bowman, K. W., Lamarque, J. F., Naik, V., Stevenson, D. S.,
852   Tilmes, S., Voulgarakis, A., Wild, O., Bergmann, D., Cameron-Smith, P., Cionni, I., Collins,
853   W. J., Dalsoren, S. B., Doherty, R. M., Eyring, V., Faluvegi, G., Horowitz, L. W., Josse, B.,
854   Lee, Y. H., MacKenzie, I. A., Nagashima, T., Plummer, D. A., Righi, M., Rumbold, S. T.,
855   Skeie, R. B., Shindell, D. T., Strode, S. A., Sudo, K., Szopa, S., and Zeng, G.: Pre-industrial
856   to end 21st century projections of tropospheric ozone from the Atmospheric Chemistry and
857   Climate Model Intercomparison Project (ACCMIP), Atmos Chem Phys, 13, 2063-2090,
858   DOI 10.5194/acp-13-2063-2013, 2013.
859 Young, P. J., Naik, V., Fiore, A. M., Gaudel, A., Guo, J., Lin, M. Y., Neu, J. L., Parrish, D. D.,
860   Rieder, H. E., Schnell, J. L., Tilmes, S., Wild, O., Zhang, L., Ziemke, J., Brandt, J., Delcloo,
861   A., Doherty, R. M., Geels, C., Hegglin, M. I., Hu, L., Im, U., Kumar, R., Luhar, A., Murray,
862   L., Plummer, D., Rodriguez, J., Saiz-Lopez, A., Schultz, M. G., Woodhouse, M. T., and
863   Zeng, G.: Tropospheric Ozone Assessment Report: Assessment of global-scale model
864   performance for global and regional ozone distributions, variability, and trends, Elementa-
865   Science of the Anthropocene, 6, 2018.
866 Zeng, G., Morgenstern, O., Braesicke, P., and Pyle, J. A.: Impact of stratospheric ozone recovery
867   on tropospheric ozone and its budget, Geophys. Res. Lett., 37, L09805,
868   10.1029/2010gl042812, 2010.
869 Ziemke, J. R., Oman, L. D., Strode, S. A., Douglass, A. R., Olsen, M. A., McPeters, R. D.,
870   Bhartia, P. K., Froidevaux, L., Labow, G. J., Witte, J. C., Thompson, A. M., Haffner, D. P.,
871   Kramarova, N. A., Frith, S. M., Huang, L. K., Jaross, G. R., Seftor, C. J., Deland, M. T., and
872   Taylor, S. L.: Trends in global tropospheric ozone inferred from a composite record of
873   TOMS/OMI/MLS/OMPS satellite measurements and the MERRA-2 GMI simulation,
874   Atmos Chem Phys, 19, 3257-3269, 10.5194/acp-19-3257-2019, 2019.
875
876